

See discussions, stats, and author profiles for this publication at: <https://www.researchgate.net/publication/279231129>

Micellization and Mobility of Amphiphilic Poly(2-oxazoline) Based Block Copolymers Characterized by ^1H NMR Spectroscopy

ARTICLE in MACROMOLECULES · JUNE 2015

Impact Factor: 5.8 · DOI: 10.1021/acs.macromol.5b00149

READS

37

5 AUTHORS, INCLUDING:



Wolf Hiller
Technische Universität Dortmund
89 PUBLICATIONS 1,015 CITATIONS

[SEE PROFILE](#)



Nadine Engelhardt
BPCN
2 PUBLICATIONS 6 CITATIONS

[SEE PROFILE](#)



Patrick Degen
Technische Universität Dortmund
48 PUBLICATIONS 201 CITATIONS

[SEE PROFILE](#)



Ralf Weberskirch
Technische Universität Dortmund
51 PUBLICATIONS 1,450 CITATIONS

[SEE PROFILE](#)

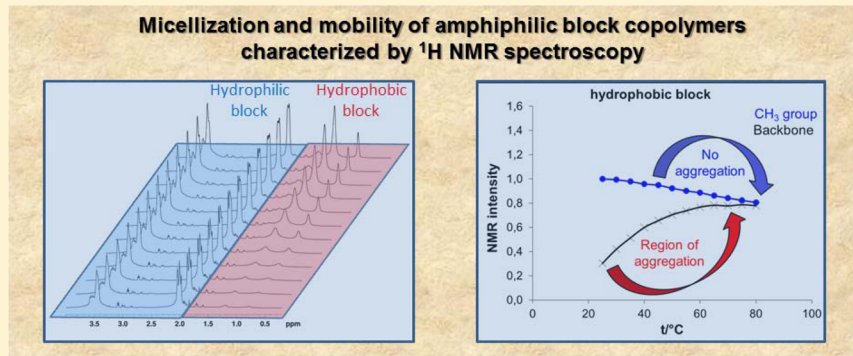
Micellization and Mobility of Amphiphilic Poly(2-oxazoline) Based Block Copolymers Characterized by ^1H NMR Spectroscopy

Wolf Hiller,^{*†} Nadine Engelhardt,[†] Anne-Larissa Kampmann,[†] Patrick Degen,[‡] and Ralf Weberskirch^{*†}

[†]Faculty of Chemistry and Chemical Biology, TU Dortmund, Otto-Hahn-Straße 6, D-44227 Dortmund, Germany

[‡]Center for Synchrotron Radiation (DELTa), TU Dortmund, Maria-Goeppert-Meyer-Str. 2, D-44227 Dortmund, Germany

Supporting Information



ABSTRACT: Three amphiphilic diblock poly(2-oxazoline) copolymers composed of the hydrophilic poly(2-methyl-2-oxazoline) and hydrophobic poly(2-alkyl-2-oxazoline) with alkyl = pentyl (**P1**), heptyl (**P2**), and nonyl side chain (**P3**) lengths of the hydrophobic block were synthesized by ring-opening cationic polymerization. These polymers form micelles in water above their critical micelle concentration. The temperature-dependent stability of the micellar aggregates was analyzed by DLS and turbidity measurements as well as pyrene solubilization between 20 and 80 °C in water. Moreover, the chemical composition of the block copolymers was determined by ^1H NMR spectroscopy. In particular, it was possible to quantify the degree of aggregations of the individual groups of both blocks by including the chemical composition into the derived equations. It could be shown by varying the temperature that both the chemical composition and the degree of micellization depend on the number of bonds of the considered structural groups of the side chain with respect to the backbone of the hydrophobic block as well as the length of the side chain. In addition, temperature-dependent T_1 and T_2 measurements were performed to determine the dynamics of the structural groups of the hydrophilic and hydrophobic blocks. Correlation times and activation energies were determined of the individual structural groups confirming the different mobilities.

INTRODUCTION

Amphiphilic block copolymers represent the most important extension of low molar mass amphiphiles with respect to structural diversity, chemical composition, and functionality. The simplest and still most abundant type of block copolymer consists of two block segments AB in a linear arrangement, each formed by a different monomer.^{1,2} In selective solvents, amphiphilic block copolymers self-assemble and can form a variety of aggregated structures including vesicles,³ polymerosomes,⁴ and micelles.⁵ Especially polymer micelles have attracted much attention in the past due to their potential application in biomedical,^{6–12} surface modification,^{13–15} and catalysis.^{16–18}

An interesting class of amphiphilic block copolymers is based on poly(2-oxazolines) that are prepared by ring-opening cationic polymerization.^{19–21,30–32} The length of the alkyl side chains controls to a large extent the solubility in water of the poly(2-alkyl-2-oxazolines). Only polymers with 2-methyl-, 2-ethyl-, and 2-isopropyl-2-oxazolines lead to water-soluble

materials at room temperature while longer alkyl side chains lead to water-insoluble polymers.²² Moreover, it has been shown that aqueous solutions of certain homopolymers such as poly(2-isopropyl-2-oxazoline) (PIPOZ) and poly(2-ethyl-2-oxazoline) (PEOZ) undergo phase separation upon heating beyond their cloud point temperature, T_{CP} . Depending on the polymer molecular weight and polymer concentration, T_{CP} ranges from 36 to 80 °C^{23,24} and from ~62 to 100 °C²⁵ for solutions of PIPOZ and PEOZ, respectively. This property has also been used to design gradient copolymers²⁶ and block copolymers²⁷ based on different IPOZ and EOZ content to study the effect of polymer composition on T_{CP} behavior and the self-association process. Because of their chemical and structural diversity and their solubilization properties, poly(2-oxazolines) have been intensively investigated in recent years

Received: January 23, 2015

Revised: May 26, 2015

Published: June 10, 2015



for their potential use in biomedical application^{28,29} and micellar catalysis.^{30–35} For the latter application, the catalyst was introduced into the hydrophobic part of an amphiphilic poly(2-alkyl-2-oxazolines) block copolymer that form nanometer sized micelles above a critical polymer concentration with the catalyst located in the core surrounded by a hydrophilic polymer shell. These catalytically active polymer micelles have been applied successfully in numerous metal-catalyzed reactions in aqueous media, with reaction temperatures in the range of 20 °C^{30,31} to 100 °C.^{32–35} Despite all the successful reactions carried out, there is still little knowledge about the temperature-dependent stability of such polymer micelles and the dynamics of amphiphilic block polymers with longer alkyl side chains in a micellar solution as a function of temperature and location in the hydrophilic shell or hydrophobic core. A deeper understanding, however, could be important for the development of new catalytically active polymer micelles with improved activity and selectivity.

A particularly interesting method to study polymer and micelle dynamics at different temperatures is NMR measurement of spin relaxation rates such as spin–lattice relaxation time T_1 and spin–spin relaxation time T_2 . They provide insights into the molecular dynamics of single moieties as a function of temperature and are highly dependent on molecular tumbling rates, which are highly dependent on the aggregation behavior of the block copolymers.^{36–39} In the past, NMR studies of polymer amphiphiles have been used to investigate the micellization of poly(ethylene oxide)-*b*-poly(propylene oxide) (PEO-*b*-PPO) block copolymers below and above the lower critical solution temperature (LCST) in aqueous media,^{40–44} the effect of chain rigidity for a series of amphiphilic poly(acrylate) block copolymers,⁴⁵ and the micellization of styrene–methyl methacrylate gradient copolymers.⁴⁶

Here we report the synthesis and the comprehensive NMR characterization of three poly(2-oxazoline) block copolymers with pentyl, heptyl, and nonyl side chains in the hydrophobic block and poly(2-methyl-2-oxazoline) as the hydrophilic block. In particular, we were interested in the characterization of polymer micelles formed in water. Therefore, we have conducted temperature-dependent NMR, DLS, pyrene solubilization, and turbidity measurements to better understand the temperature-dependent stability of such polymer micelles. In particular, we have carried out quantitative ^1H NMR measurements as well as T_1 and T_2 relaxation NMR experiments in deuterium oxide above the critical micelle concentration (CMC). With the aid of these experiments we will obtain quantitative information about chemical compositions, degree of aggregations, and dynamics of the individual functional groups of the polymer backbone and the alkyl side chains. It will be shown how the degree of aggregations can be determined by including the chemical composition of the copolymer. The results provide excellent insights into the polymer composition and dynamics upon micellization as a function of temperature and the pendent alkyl chain length.

EXPERIMENTAL SECTION

Materials and General Methods. All substances required for the monomer and polymer synthesis were purchased from Sigma-Aldrich (Steinheim, Germany), Acros (Nidderau, Germany), and ABCR (Karlsruhe, Germany). They were used as received unless otherwise stated. Dry solvent were purified by a purification system M Braum glovebox Technology PLC 800. Methyl triflate (MeOTf), 2-methyl-2-

oxazoline (MeOx), and acetonitrile (ACN) for polymer preparation were dried by refluxing over CaH_2 under a dry nitrogen atmosphere and subsequent distillation prior to use.

Polymer Synthesis. All polymerizations were carried out in a Schlenk tube under inert atmosphere (argon) using freshly distilled and dried solvents. To a solution of methyl triflate (0.59 mmol, 1 equiv) in acetonitrile (5 mL), 1.0 g of 2-methyl-2-oxazoline (11.75 mmol, 20 equiv) was added. The reaction mixture was stirred at 120 °C for 2 h. Subsequently, 2-alkyl-2-oxazoline (5 equiv) was added and polymerized at 110 °C for 4 h. At room temperature piperidine (3 equiv) as terminating agent was added, and the reaction mixture was stirred overnight. The solvent and remaining excess of piperidine were removed at reduced pressure. The solid residue was dissolved in chloroform, and potassium carbonate was added. The mixture was stirred for 3 h at RT. After filtration, the polymer was purified by precipitation in cold ether. The precipitated polymer was obtained by centrifugation.

A detailed description of the monomer synthesis including the analytical analysis with NMR, mass spectrometry, size exclusion chromatography, light scattering, and fluorescence spectroscopy are given in the Supporting Information.

NMR Experiments. The NMR experiments were performed with a 500 MHz spectrometer DD2-500 from Agilent Technologies equipped with a 5 mm triple resonance probe H(C,X). The measurements of the aggregations, chemical compositions, and T_1 and T_2 relaxation times were carried out at concentrations of 15 mg/0.6 mL using deuterium oxide as solvent. This concentration is above the critical micelle concentration. The T_1 relaxation times were measured with the inversion recovery method. The T_2 measurements were performed with the Curr–Purcell–Meiboom–Gill pulse sequence.^{47,48} The 90° pulse was 9.5 μs and the τ interval 1 ms. The acquisition time was 4.09 s, spectrum width of 4325 Hz, 35 kb data, and the relaxation delay of 10 s. Up to 14 different delays were chosen to cover the magnetization of the T_1 and T_2 experiments. Eight transients were accumulated per free induction decay. The temperature range was varied between 25 and 80 °C in steps of 5 °C. The actual temperatures of the NMR experiments were calibrated with ethylene glycol.

Dynamic Light Scattering. The dynamic light scattering experiments were performed using the Zetasizer Nano Instrument (Malvern). A 4 mW He–Ne laser (633 nm wavelength) with a fixed detector angle of 173° was used for these measurements. About 1 mL of the dust-free sample was transferred to a special light scattering cell. The experiments were started 10 min after the desired temperature (20–80 °C) was reached to allow the temperature to equilibrate. The temperature was controlled within a tolerance of ± 0.02 °C, and for each temperature, the measurements were repeated five times. For further interpretation, we used the average values of these five measurements.

Fluorescence Intensity Measurements. The static fluorescence intensity measurements were carried out with a PerkinElmer luminescence spectrometer LS 55. Fluorescence emission spectra of pyrene in the polymer solution were recorded by using an excitation wavelength of 334 nm. In these spectra, fluorescence intensities were measured at 373 nm (peak 1) and 384 nm (peak 3). From a stock solution of pyrene in methanol, a known volume was transferred into the aqueous polymer solutions; the final pyrene concentration was 5×10^{-6} M. Before starting the fluorescence measurements oxygen was removed from the samples by agitation with argon.

RESULTS AND DISCUSSION

Polymer Synthesis and Characterization. The amphiphilic block copolymers have been prepared by the living cationic ring-opening polymerization of 2-oxazolines according to well-established literature procedures.²⁰ Therefore, 2-methyl-2-oxazoline was used to synthesize the hydrophilic block while different 2-alkyl-2-oxazolines (alkyl = pentyl, heptyl, and nonyl) were used to form the hydrophobic block. We decided to prepare rather short polymers with a length for the hydrophilic

Scheme 1. Synthesis of the Amphiphilic Block Copolymers P1–P3

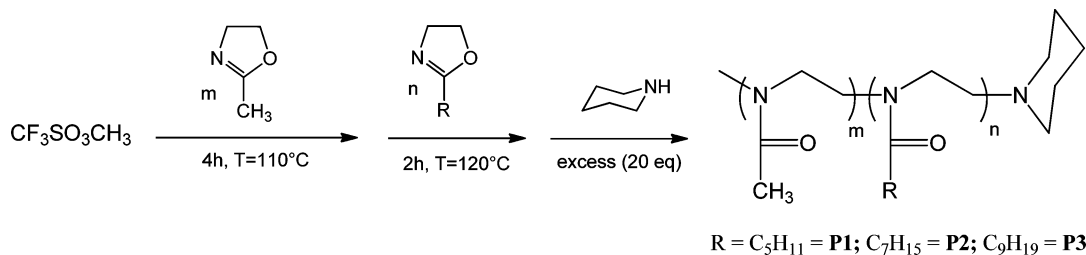


Table 1. Analytical Data of the Polymers P1, P2, and P3

polymer	$m:n_{\text{exp}}$	$^1\text{H NMR}^a$	$m:n$	M_n^a (g mol $^{-1}$)	PDI b	cmc c (mol L $^{-1}$)	d (z-average) d (nm)
P1	17:3		5.6	1970	1.18	6.5×10^{-7}	9.4 ± 0.25
P2	16:4		4.0	2140	1.18	2.5×10^{-7}	11.3 ± 0.3
P3	17:4		4.25	2340	1.17	6.0×10^{-8}	15.2 ± 0.42

^aChemical composition and molar mass were determined by ^1H NMR spectroscopy and end-group analysis, respectively. ^bPolydispersity indices (PDI) were obtained by SEC with polystyrene standards in DMF/0.1% LiBr. ^cCritical micelle concentration (cmc) was determined by pyrene solubilization experiments of P1–P3 at different polymer concentrations in aqueous media based on I_1/I_3 measurements. ^dDiameter (z-average) was determined by DLS measurements of polymer solutions (15 mg/0.6 mL H₂O) in water at RT.

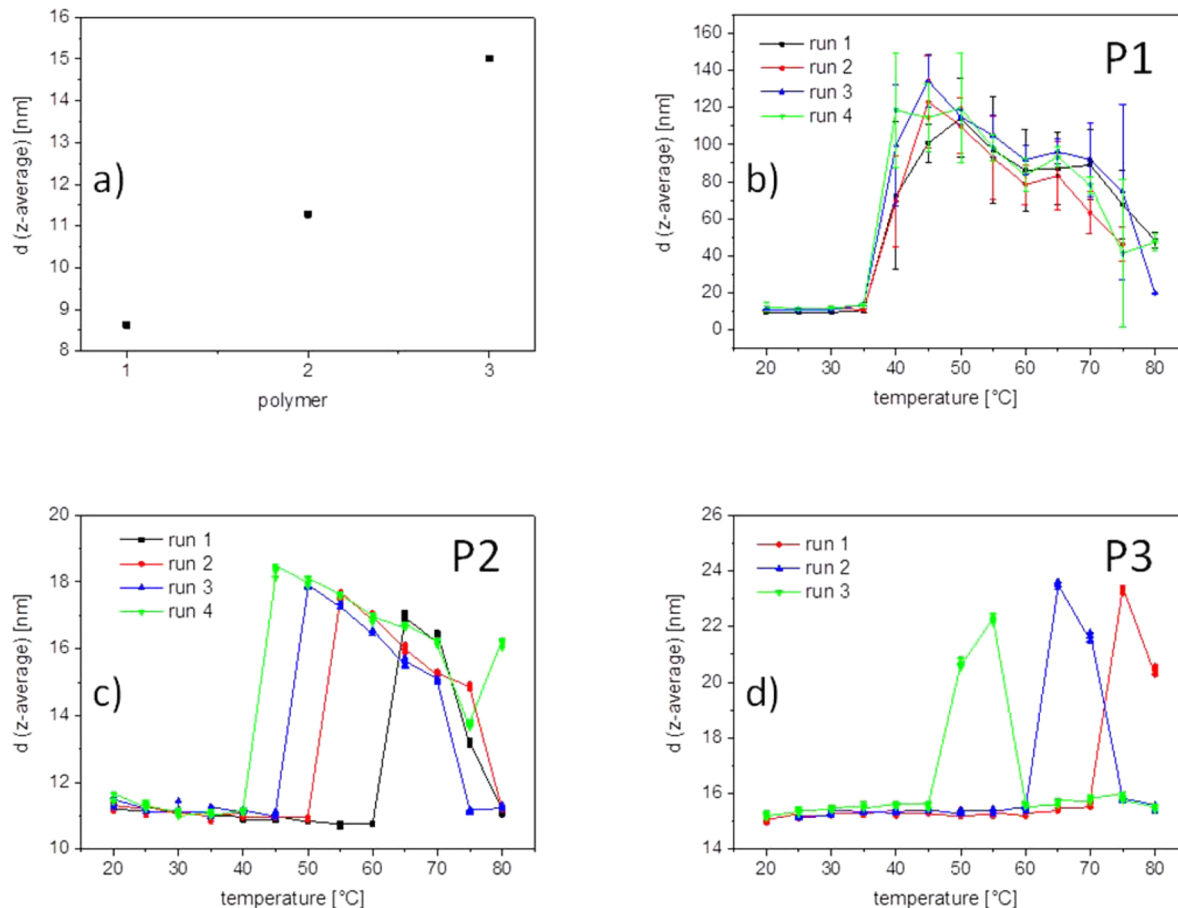


Figure 1. (a) DLS measurements for P1–P3 at 20 °C; temperature dependence of average hydrodynamic diameter for polymer micelles based on P1 (b), P2 (c), and P3 (d), all at 15 mg/0.6 mL H₂O.

block of \sim 17 monomer units and \sim 4 repeating units in the hydrophobic block since similar block copolymers have been used in the past in various micellar catalysis applications.^{30–35}

The polymers P1–P3 were analyzed by ^1H NMR spectroscopy to determine the polymer composition. Moreover, the end-group analysis and SEC measurements were used to determine the molar masses and polydispersity of the polymers.

The tendency of poly(2-methyl-2-oxazoline)-*b*-poly(2-alkyl-2-oxazolines) to form micelles in aqueous media has been reported in several publications.^{30–35} Steady-state fluorescence spectroscopy and in particular the solubilization of pyrene were applied to determine the critical micelle concentration (cmc) of the amphiphilic polymer P1 to P3 in water. CMC values were in the micromolar range and decreased from P1 to P3 with

increasing length of the alkyl side chain from pentyl to nonyl groups. Moreover, the size of the aggregates as analyzed by dynamic light scattering showed particle diameters between 9.4 and 15.2 nm from **P1** to **P3** increasing with increasing length and were in excellent agreement with previous reports of poly(2-oxazoline) block copolymers of similar composition.^{30,34} The analytical data are summarized in Table 1.

Temperature Dependent DLS and Fluorescence

Probe Measurements. Dynamic light scattering was used to analyze temperature-dependent changes of particle sizes and also gain deeper insight into the temperature stability of the micellar aggregates. Therefore, we measured the particle size of the aqueous polymer solutions between 20 and 80 °C in intervals of 5 °C (see Figure 1). The solution of **P1** showed a rather constant particle size between 20 and 35 °C that sharply increased at 40 °C to nearly 120 nm. With increasing temperature to 80 °C the particle size decreased again and remained at ~50 nm at 80 °C. This behavior was reproducible in four consecutive runs showing always a very similar particle size–temperature dependency with a maximum particle size of 115–135 nm that was always observed between 40 and 50 °C (see Figure 1b). While the temperature dependence of the micellar sizes for **P2** looks similar, two distinct differences can be observed. First, the increase in particle size with increasing temperature is only around 50% and particle size increased from ~11 nm to around ~18 nm while in the case of **P1** the particle size increased by around 1300%. Second, the onset temperature of particle size increase is decreasing from 65 to 45 °C from the first to the fourth run for **P2** (see Figure 1c). The behavior of **P3** resembles that of **P2**. The sharp increase in particle size took place in the first run at 75 °C and is shifted to 50 °C in the third run. Particle sizes increase for **P3** to ~50% (see Figure 1d). We ran also a DLS analysis with a block copolymer based on DMAA and styrene in water at the same concentration in the same temperature range to make sure not seeing any artifacts. The particle size remained nearly constant over the whole temperature range from 20 to 80 °C with a diameter of ~22.6 nm (see Figure S1).

As mentioned before, it is well-known that aqueous solutions of certain poly(2-oxazoline)s display cloud point temperatures that are easily tunable over a wide range of temperatures and depend on molecular weight and polymer concentration. Such temperature-sensitive behavior has been only reported for homo- and copolymers where at least one component was 2-ethyl-2-oxazoline (EOx),^{23,24,49} 2-isopropyl-2-oxazoline (iPropOx),^{25,50–52} or 2-n-propyl-2-oxazoline (PropOx).⁴⁹ Since the block copolymers **P1**–**P3** do not contain any of these oxazoline monomers, the temperature-sensitive micellar size dependency was difficult to understand. Poly(2-methyl-2-oxazolines) have been reported to be too hydrophilic to show any cloud point temperature while poly(2-alkyl-2-oxazolines) are known to be too hydrophobic and nearly water-insoluble. Turbidity measurements for the micellar solutions of **P1**–**P3** did not show any change in transmittance over the whole temperature range (see Figure S2), suggesting that no larger aggregates are formed during the heating process which is very typical for homopolymers and very often also for copolymers that display a cloud point temperature. However, a recent work by Hoogenboom and Kjønigsen showed that block copolymers consisting of a 2-ethyl-2-oxazoline block and a block consisting of a random copolymer of 2-ethyl-2-oxazoline and 2-n-propyl-2-oxazoline (PEtOx-block-P(EtOx-stat-PropOx)) can display also a more complex temperature-dependent aggregation

behavior.⁴⁹ With increasing temperature they observed an increase in particle size by DLS measurements due to the increased hydrophobicity of their copolymer accompanied by a sharp decrease in transmittance, suggesting the formation of larger aggregates. When the temperature was further increased, the aggregates size decreased again by a factor of ~10. This effect has been explained by partial dehydration of the EtOx block and possibly also fragmentation of the aggregates.⁴⁹ Depending on the copolymer composition, the temperature dependent increase in particle size did not lead to a decrease of transmittance which was explained by a swelling effect of the aggregates rather than the formation of larger aggregates. While this observation is very similar to what we observe for our block copolymer micelles, it remains unclear why the temperature-induced change in micelle size can be observed for block copolymers that do not contain any 2-oxazoline monomer that have been identified in the past to display a cloud point. Moreover, Papadakis et al. investigated the micelle formation of poly(2-methyl-2-oxazoline)-block-poly(2-nonyl-2-oxazoline) labeled with a tetramethyl rhodamine (TRITC) probe by photon correlation spectroscopy (PCS) and fluorescence correlation spectroscopy (FCS).⁵³ They found larger, metastable aggregates that disappeared after a first annealing step. The formation of these aggregates was attributed to the alkyl side chain crystallization and was not detected anymore in consecutive runs. However, it is difficult to compare the data since the copolymer composition analyzed was quite different from our closest polymer **P3**. Moreover, it remains unclear what effect TRITC may have on the temperature-dependent aggregation behavior of such copolymers.

Based on the report by Hoogendoom, there might be the possibility that particle swelling takes place with increasing temperature and thus resulting in larger particles.⁴⁹ Such an effect would change the micropolarity of the micellar core that can be probed by static fluorescence measurements and pyrene solubilization. The emission spectra of pyrene are characteristic of monomer fluorescence in specific microenvironments, where the ratio of the intensity of the first and third vibronic peaks, I_1/I_3 , can be used to monitor pyrene micropolarity and the formation of hydrophobic domains.⁵⁴ The polymers **P1**–**P3** were all studied at a fixed concentration of 15 mg/0.6 mL H₂O well above their individual cmc. As can be seen in Figure 2, the I_1/I_3 values at 20 °C were 1.42 (**P1**), 1.33 (**P2**), and 1.18 (**P3**)

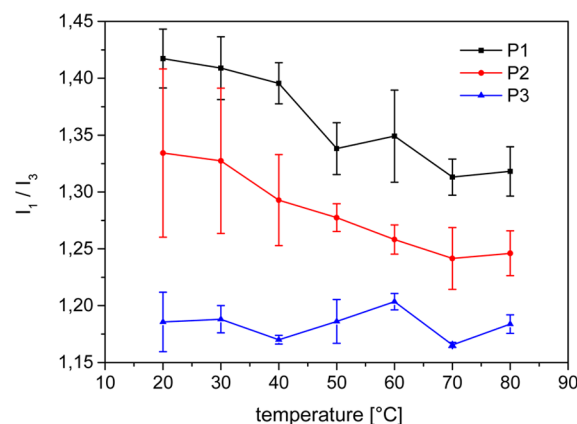


Figure 2. I_1/I_3 as a function of temperature obtained for **P1**–**P3** (15 mg/0.6 mL H₂O). Pyrene concentration was fixed at 5.0×10^{-7} mol/L in all cases.

which are typical values for such block copolymer micelles, suggesting that pyrene is solubilized in the micellar core.⁵⁵ With increasing side chain length the value of I_1/I_3 decreased from 1.42 for **P1** to 1.18 for **P3** at room temperature, suggesting an increase in hydrophobicity in the micellar core with increasing length of the hydrophobic side chain.

Moreover, P1 and P2 show also some temperature dependency and decreasing I_1/I_3 values with increasing temperature while this was not observed for P3. The decreasing I_1/I_3 values can be attributed to an increase in hydrophobicity experienced by pyrene with increasing temperature. One reason for this may be the increased side chain flexibility with increasing temperature, as can be also seen by the NMR data in Figure 9 (T -dependent aggregation) and Figure 10 (T -dependent T_1 values), that may support the solubilization of pyrene in the hydrophobic core. The results confirm the findings from the DLS measurements that the particles remain intact in the investigated temperature range between 20 and 80 °C. Moreover, the rather constant or slightly decreasing I_1/I_3 values with temperature do not support the hypothesis of any swelling of the micellar core.

Another possible explanation for the temperature-sensitive behavior observed for P1–P3 may be a combination of two effects that are all known to decrease a cloud point temperature. The first effect is the block copolymer structure and the fact that hydrophobic comonomers led to a decrease in T_{CP} for polymers based on 2-ethyl-2-oxazoline or 2-isopropyl-2-oxazoline.⁵⁶ The second effect may be due to the high local concentration of the poly(2-methyl-2-oxazoline) block in the micellar shell since it is well-known that the cloud point depends also on the polymer concentration and composition. Increased copolymer concentration and hydrophobic components are known to lower any possible cloud temperature.⁵⁶ To understand better the temperature-dependent aggregation behavior and polymer dynamics, we studied the hydrophilic block and the hydrophobic block with the alkyl side chains of each polymer micelle from P1 to P3 by NMR measurements.

3. NMR Analysis of Amphiphilic Copolymers. After the structural elucidation of the NMR spectra, ^1H NMR spectroscopy is used to characterize the degree of aggregation and also the chain dynamics of the polymer micelles formed by the amphiphilic copolymers **P1–P3**. For the first time it will be shown how the chemical composition of the block copolymers can be used to determine the degree of aggregation. In particular, the normalized intensities of the ^1H NMR signals will be analyzed with respect to the aggregation behavior of the hydrophilic and hydrophobic blocks. Furthermore, the aggregation behavior will be compared to the dynamics of both blocks analyzed by T_1 and T_2 measurements in dependence of the temperature. The results will directly reveal the influence of the side chains length of the hydrophobic block on the degree of aggregation as well as the different mobilities of the structural groups.

First, the polymers P1–P3 were characterized by ^1H NMR. The assignments of the signals to the different chemical moieties of these polymers are shown in Figure 3. This figure shows the ^1H spectrum of P1 dissolved in methanol. Methanol was chosen as a nonselective solvent that prevents aggregate formation and provides fully dissolved polymers. Consequently, the true chemical composition of the hydrophilic and hydrophobic blocks could be accurately determined. The quantified ^1H NMR spectra of P1, P2, and P3 in methanol are shown in Figures S3, S4, and S5. The hydrophilic block is

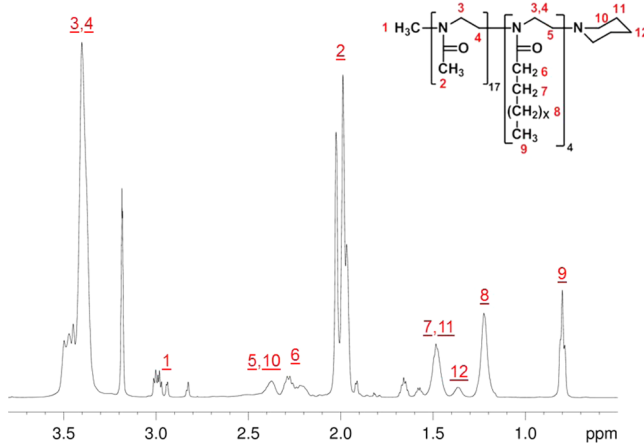


Figure 3. ^1H NMR spectrum of P(MetOx) $_{17-b}$ -(PentOx) $_3$ **P1** (with $x = 2$) in methanol.

mainly characterized by the methyl group 2 while the hydrophobic block is given by the side chains containing the methylene groups 6, 7, and 8 as well as the methyl group 9. The integral of signal 8 versus 6, 7, or 9 provides directly the length of the side chain. The main chain methylene groups 3 and 4 belonging to both blocks are completely overlapping. In addition, the CH₃ end group 1 as well as the CH₂ groups of the piperidine end group 10, 11, and 12 were also identified. The assignments of the individual groups could be performed on the basis of two-dimensional NMR spectra shown in Figures S6–S9.

3.1. Quantification of Aggregation and Chemical

Composition. In the following the behavior of the NMR intensity of the hydrophilic and hydrophobic blocks, the average chemical compositions of the copolymers, the formation of aggregations, and the dynamics of the individual structural groups will be studied in deuterium oxide solutions. As has been shown before by fluorescence measurements and DLS analysis, the aggregates formed by the polymer P1–P3 are supposed to be micellar structures. Temperature-dependent NMR measurements were performed, and analytical equations were derived to obtain quantitative data of the aggregation and dynamics for each individual structural moiety of each block copolymer in the micellar state.

First, the NMR intensities were recorded in dependence on the temperature. Figure 4 and Figures S10 and S11 show temperature-dependent ^1H NMR spectra of the three amphiphilic block copolymers **P3**, **P2**, and **P1**, respectively. In particular, Figure 4 is clearly showing the strong influence of the temperature on the changing intensities of the side chain groups C6, C7, C8, and C9 for sample **P3** in comparison to the backbone and hydrophilic group.

These spectra of Figure 4 as well as Figures S10 and S11 allow for proton normalized integrations. Figures 5 and 6 show the normalized integral intensities of individually assigned signals of the hydrophilic and hydrophobic blocks of samples P1–P3.

Only the methyl groups of samples P1–P3 show the expected linear decrease of the NMR intensities as typically observed for nonaggregated samples. This behavior is demonstrated by the linear red curves of the COCH_3 group in Figures 5a–3c for all three samples. The backbone NCH_2 group of the hydrophilic block is differently behaving. The linear range of the NCH_2 group is achieved at different

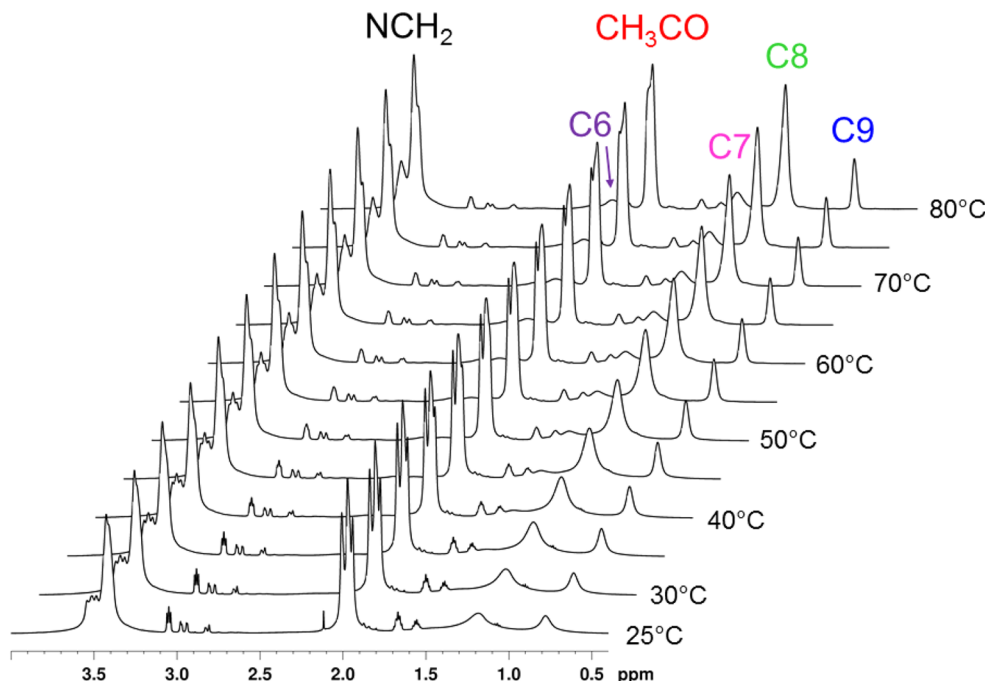


Figure 4. ^1H NMR spectra (in D_2O) in dependence of the temperature for sample P3.

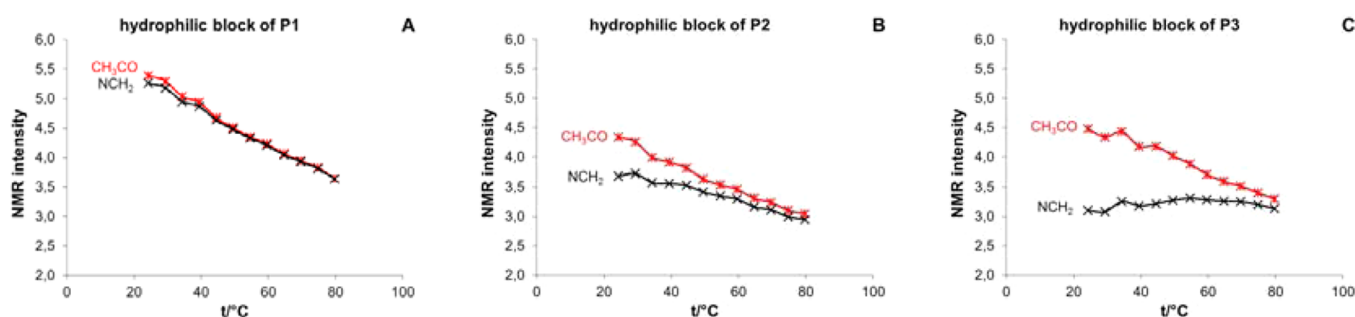


Figure 5. NMR intensities normalized to one proton of the CH_3CO side group and the NCH_2 backbone protons of the hydrophilic blocks of P1–P3.

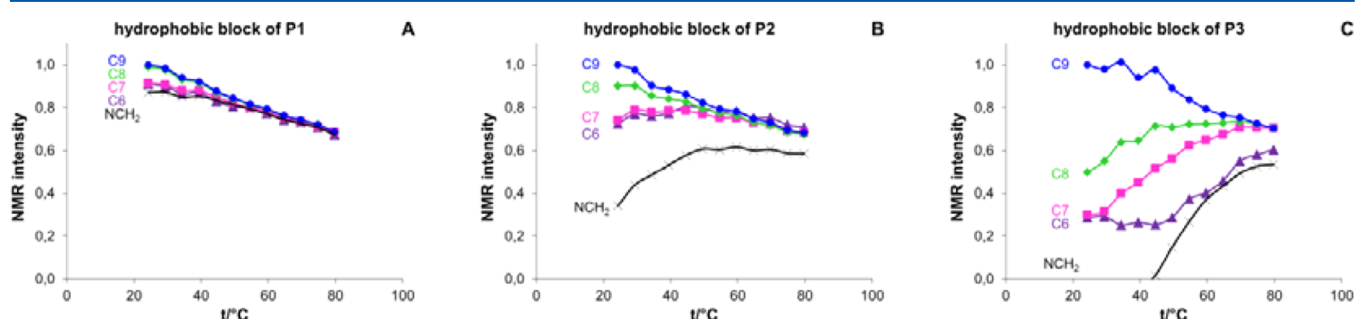


Figure 6. NMR intensities normalized to one proton of the CH_2 and CH_3 groups of the alkyl side chains and the NCH_2 backbone protons of the hydrophobic blocks of P1–P3.

temperatures. P1 reaches the nonaggregated region for this CH_2 group at about 40°C , P2 at about 60°C , and P3 above 80°C . This figure clearly indicates that the backbone of the hydrophilic block experiences the restricted mobility caused by the formation of hydrophobic aggregations. However, the typical nonaggregated linear behavior is still found for all three amphiphilic copolymers by considering the CH_3CO group. This group mainly represents the hydrophilic block and is not forming aggregates.

Figure 6 clearly reveals the formations of aggregations of the hydrophobic moieties by showing strong deviations from the linear intensity functions. In particular, the influence of the side chain length is obvious. First, the longer the side chain the stronger the formation of aggregation of a certain moiety. Second, the larger the number of bonds from the backbone to the studied side chain group, the weaker is the formation of aggregations. This tendency is observed for the groups C6, C7, C8, and C9 of samples P1–P3. The CH_3 end group of the side

chain C9 is not aggregated at all for all samples indicated by the linear temperature behavior. The other groups show clear tendencies of the aggregations in respect to the length of the side chain and the distance to the backbone. The formation of aggregation is represented by the deviations of the intensity curves in comparison to the linear decreasing function (comparison to C9). Therefore, the strongest formation of aggregations experiences C6 which is the closest group to the backbone. This behavior is demonstrated in Figure 6 by the strongest deviations from the linear decreasing intensity curve. Moreover, this influence is significantly increasing with the increase of the side chain length. Whereas C6 of P1 reaches the dissolution of the aggregation at about 40 °C, C6 of P2 reaches this status at about 60 °C, and in the case of P3 the aggregations are dissolved above 80 °C. The next weaker formation of aggregations is measured for C7 followed by C8. However, similar aggregation behavior of C6, C7, and C8 is observed by comparing P1–P3: the strength of aggregations is increasing in dependence of increasing side chains. The backbone NCH₂ groups of the hydrophobic block, however, form the strongest aggregations. Again, the influence on the aggregations increases also with larger side chains. In the case of P3 the NCH₂ groups even show negative intensities due to the calculation procedure. These protons completely overlap with the hydrophilic NCH₂ protons. Therefore, the calculation of the hydrophobic part is based on the difference of the total peak and the corresponding hydrophilic CH₃CO protons. Because of the fact that the hydrophilic NCH₂ protons of P3 already experience the restricted mobility of the hydrophobic block, the intensity of these protons is smaller than the intensity of complete nonaggregated protons. As a consequence the difference will be negative. In any case, it can already be concluded that the hydrophobic block tends to strong aggregate formations with distinct differences for each methylene/methyl group of the alkyl side chains while the hydrophilic block is not forming aggregates and shows only a reduced mobility for the backbone. Furthermore, sample P3 with the longest side chain also forms the strongest aggregations, while P1 with the shortest side chain shows the weakest formation of aggregates.

To confirm these results, we want to quantify the aggregations. Therefore, equations will be derived for allowing the calculation of the amount of aggregations in dependence of the temperature. According to Spevacek et al.,^{57–60} the degree of associations of PMMA can be determined by the ratio of intensities of the completely nonassociated polymer and nonassociated parts with coexisting associated regions. He demonstrated that the completely nonassociated bulk polymer shows a linear decrease of the NMR intensity with increasing temperature. Deviations of the linearity are related to the existence of associations. This method will be adopted now for the investigation of amphiphilic block copolymers. In this case the degree of aggregations should be calculated for both blocks separately. This model assumes that high-resolution liquid NMR provides lower intensities for block copolymers with regions of micelles due to the restricted mobility of such aggregates. Consequently, the quantification of the micellar aggregations at a certain temperature is given by the intensity of the copolymer without any micelle aggregations and the observed intensity. The latter one is supposed to be the measurement of the nonaggregated part of the copolymer in the presence of aggregated micelles with restricted mobility. Thus, the following equations are proposed for the calculation

of the degree of aggregations of the hydrophobic and hydrophilic block and determine the degree of aggregations formed by micellization:

$$p_i^{hp} = \frac{I_{0,i}^{hp} - I_i^{hp}}{I_{0,i}^{hp}} \quad (1)$$

$$p_i^{hl} = \frac{I_{0,i}^{hl} - I_i^{hl}}{I_{0,i}^{hl}} \quad (2)$$

where $I_{0,i}^{hp}$ and $I_{0,i}^{hl}$ are intensities of the nonaggregated parts of the hydrophobic (index *hp*) and hydrophilic (index *hl*) blocks at the temperature *i*. These intensities decrease linearly with increasing temperature and correspond to the status without aggregations at all. I_i^{hp} and I_i^{hl} are the intensities of the observed nonaggregated parts of the hydrophobic (index *hp*) and hydrophilic (index *hl*) blocks in the presence of aggregated parts at the temperature *i*.

The intensities I_i are the intensities shown in Figures 5 and 6. As long as the nonaggregated intensities $I_{0,i}$ can be determined, the degree of aggregations can be calculated for the complete temperature range from 25 to 80 °C. The nonaggregated intensities $I_{0,i}$ can be usually obtained by generating an extrapolated asymptotic line from the linear high temperature region where the aggregations are decomposed to the required temperature. This approach is actually possible for the hydrophilic CH₃CO groups of samples P1–P3 as seen in Figure 5. In this case the temperature dependences of the signal intensities of the CH₃CO groups show even a completely linear behavior for all three samples. Consequently, $I_{0,i}^{hl}$ and $I_{0,i}^{hp}$ can be directly determined from the linear regression of these temperature dependences. In case of the hydrophobic blocks, this kind of calculation procedure of $I_{0,i}^{hp}$ can only be applied for C9 for all samples. Some temperature curves still allow for the determination of $I_{0,i}^{hp}$ via the asymptotic approach (such as C6, C7, and C8 of P1 and P2). All other temperature curves of the hydrophobic groups do not provide the asymptotic access (see C6, C7, C8, and NCH₂ of P3 in Figure 6c). Therefore, another approach will be proposed for calculating $I_{0,i}^{hp}$ using the nonaggregated chemical composition of the two blocks. The molar chemical composition $X_{0,i}^{hp}$ of the completely nonaggregated hydrophobic block is given by

$$X_{0,i}^{hp} = \frac{I_{0,i}^{hp}}{I_{0,i}^{hp} + I_{0,i}^{hl}} \quad (3)$$

with $X_{0,i}^{hl} = 1 - X_{0,i}^{hp}$ as the molar chemical composition of the totally nonaggregated hydrophilic block.

The molar chemical composition X_i^{hp} of the hydrophobic block in the presence of aggregations is then given by the temporary measured intensities of both blocks:

$$X_i^{hp} = \frac{I_i^{hp}}{I_i^{hp} + I_i^{hl}} \quad (4)$$

with $X_i^{hl} = 1 - X_i^{hp}$ as the molar chemical composition of the nonaggregated hydrophilic block in the presence of aggregations of the hydrophobic block.

Finally, the unknown intensity of the totally nonaggregated hydrophobic block can be calculated via the chemical composition of the nonaggregated hydrophobic block by solving eq 3:

$$I_{0,i}^{hp} = \frac{I_{0,i}^{hl} X_{0,i}^{hp}}{1 - X_{0,i}^{hp}} \quad (5)$$

This approach will be successful due to the fact that the chemical composition $X_{0,i}^{hp}$ of the nonaggregated hydrophobic block can be determined either by a simple measurement in methanol or at 80 °C in water where all aggregations are dissolved. Furthermore, the intensity $I_{0,i}^{hl}$ can be determined from Figure 5 with the asymptotic method. Therefore, the chemical compositions and finally the aggregations can be determined at every temperature. The high precision of this method is demonstrated in Figure 7 where the calculated $I_{0,i}^{hp}$

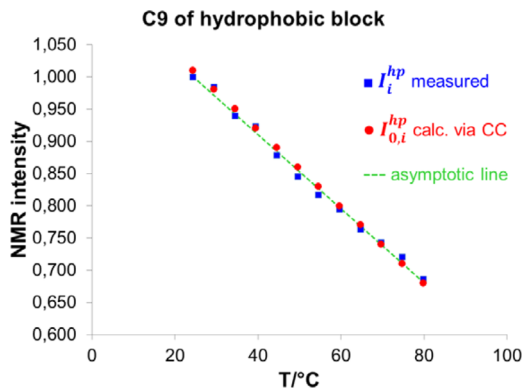


Figure 7. Determination of the nonaggregated intensities of the hydrophobic C9 group of sample P1 by using the asymptotic method and the calculation via chemical composition (CC).

values could also be verified by the asymptotic approach using the experimental data of the C9 curve of Figure 6a. The calculated $I_{0,i}^{hp}$ values perfectly match the asymptotic line as shown in Figure 7.

Based on these approaches, the chemical compositions and the aggregations were calculated for the three amphiphilic block copolymers P1–P3. Figure 8 shows the temperature dependence of the chemical compositions of the hydrophobic blocks calculated with eq 4 by using the hydrophilic signal intensities of the CH_3CO group. The content of the hydrophilic block is simply given by the sum to 100% and is not shown. Figure 9 demonstrates the temperature dependence of the aggregations for the hydrophobic and hydrophilic structural groups calculated via eqs 1, 2, and 5.

It is visible from Figure 8 that the hydrophobic moieties exhibit different temperature behaviors for each polymer P1 to P3. The changes are dependent from both the length of the

side chain and the number of bonds with respect to the backbone. The strongest changes are found for P3, followed by P2, and finally the weakest changes are found for P1. With respect to the distance of the groups to the backbone, the NCH_2 groups show the biggest changes of the chemical composition, followed by the order C6, C7, and C8, and the weakest influence is observed for C9. In particular, it is seen in Figure 8 that the correct chemical composition referring to the nonaggregated copolymers (about 16–18 mol % for the hydrophobic block) is reached at about 80 °C for all different structural groups of the side chain. The deviations found for some groups are referred to measurement errors of small signals such as C6 or overlapping peaks with other signals as observed for C7 which was finally corrected. The negative behavior of the NCH_2 is simply caused by the same calculation procedure as explained above. Since the NCH_2 peak consists of both the hydrophilic and hydrophobic parts, the hydrophobic content was calculated by subtracting the adequate number of hydrophilic CH_3CO protons. Because of the fact that the hydrophilic NCH_2 protons also experience reduced intensities affected by the reduced mobility of the strong aggregation of the hydrophobic block, this difference can be negative and the calculation of the chemical composition yields negative data.

The discussions with respect to formation of aggregations of the hydrophilic and hydrophobic blocks can be seen much clearer in Figure 9. The hydrophilic block is represented by the COCH_3 group. The hydrophobic block is given by C6, C7, C8, C9, and NCH_2 . It is very obvious from this figure now that only the hydrophobic block is forming aggregations while the hydrophilic block provides no aggregations. This is true for all three copolymers. It is also well revealed from this figure that the degree of the aggregations of the hydrophobic block depends on the bond distances to the backbone. The backbone itself (NCH_2) exhibits the strongest aggregations followed by the next neighboring CH_2 group of the side chains given by C6 and succeeded by C7, C8, and C9. The hydrophilic block represented by the CH_3CO group shows no aggregations. Figure 9 also shows the temperatures of complete decompositions of the aggregations for all structural groups. This point is given by the degree of aggregation $p_i = 0$. In the case of samples P1–P3 this temperature is about 80 °C if all groups are considered. The end group C9, however, is nonaggregated at each measured temperature and for all samples. The other groups reach the solvated state at higher temperatures if they are closer to the backbone. In these cases it could be verified that a certain group of P3 shows the stronger aggregations than P2 followed by P1 with the weakest aggregations. Accordingly, the length of the side chain obviously affects the strength of the

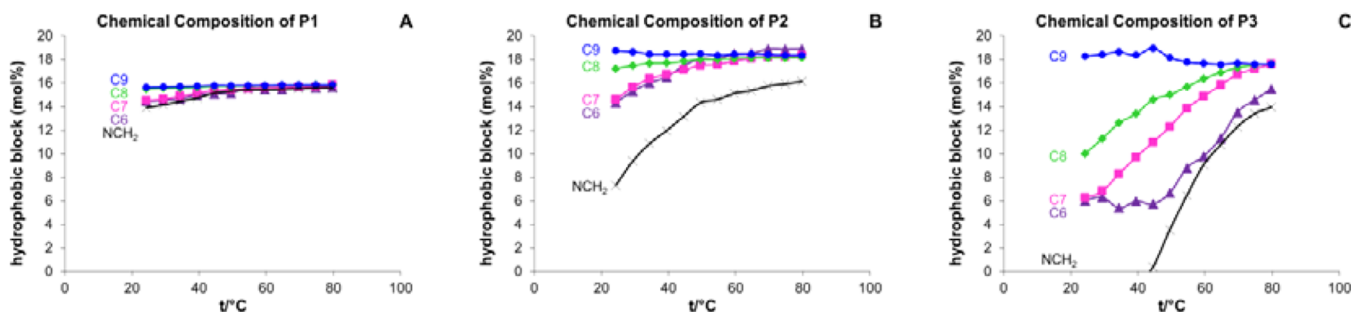


Figure 8. Temperature dependence of the chemical compositions of the amphiphilic copolymers P1–P3 showing the mol % of the hydrophobic block elements.

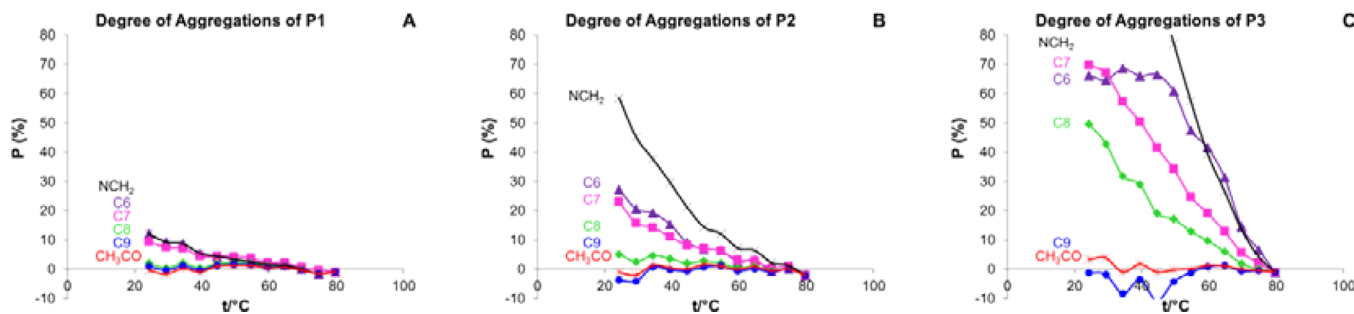


Figure 9. Temperature dependence of the aggregations of the amphiphilic copolymers **P1–P3**. The hydrophilic block is only represented by the CH_3CO groups. All other groups refer to the hydrophobic blocks.

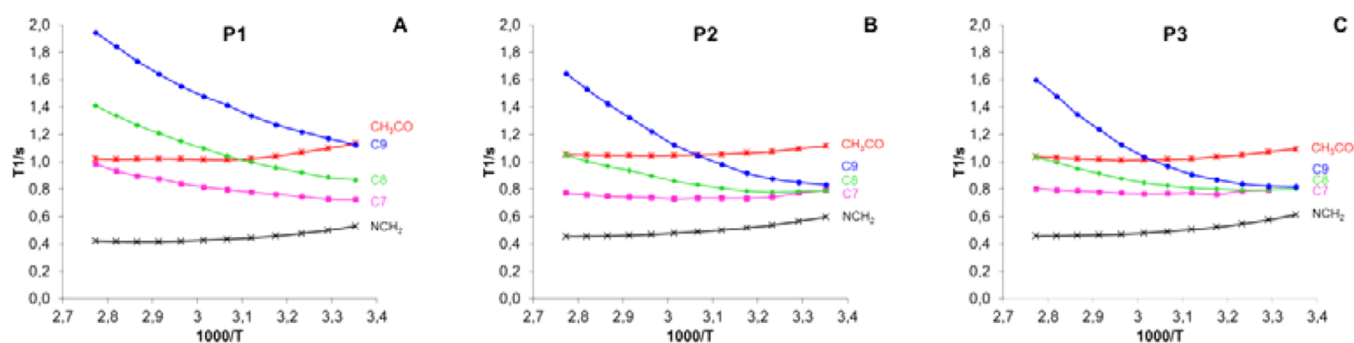


Figure 10. Temperature dependence of T_1 of samples **P1–P3** at 500 MHz. The T_1 data are recorded for the side chains (C7, C8, and C9), COCH_3 , and backbone NCH_2 groups.

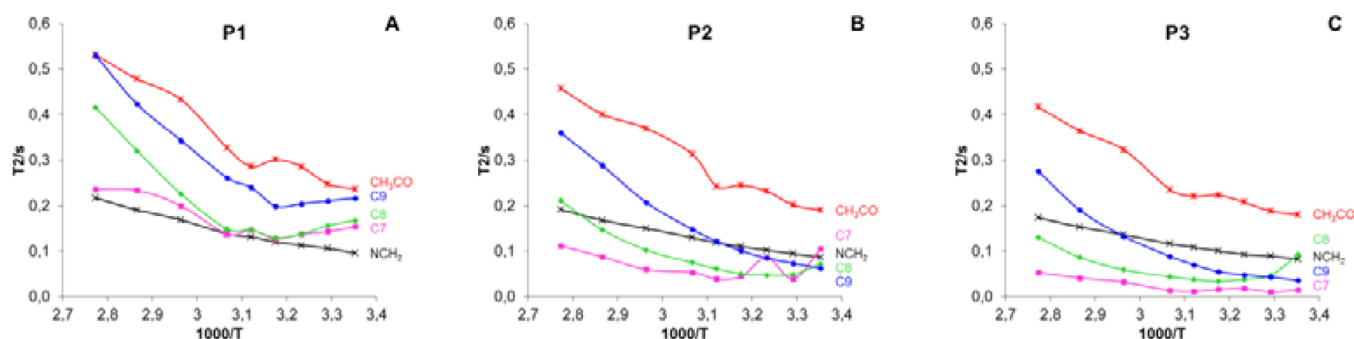


Figure 11. Temperature dependence of T_2^* of samples **P1–P3** at 500 MHz. The T_2 data are recorded for the side chains (C7, C8, and C9), COCH_3 , and backbone NCH_2 groups.

aggregation as well. The increasing side chain length also causes an increase of the degree of aggregation for a considered structural group.

3.2. Dynamics of Amphiphilic Block Copolymers. Longitudinal relaxation times T_1 and transversal relaxation times T_2 were measured in dependence of temperature to evaluate the mobility of the different components of the hydrophilic and hydrophobic parts of the copolymers. The T_1 measurements were performed by using the inversion recovery technique. The magnetization curves provided single exponential decays. Consequently, T_1 data could be directly calculated. Figure 10 shows the temperature dependence of T_1 of samples **P1–P3**. The T_2 measurements were performed with the CPMG pulse sequence in order to suppress J coupling effects. In this case the magnetization decays of the hydrophilic groups (COCH_3 and NCH_2) were exponential, while the magnetization decays of the hydrophobic groups (C7, C8, and C9) provided biexponential decays consisting of a short and a long component. The nonexponential analysis using eq S1 is demonstrated in Figures

S12–S15. In order to obtain smoother exponential T_2 data for the temperature simulation, an averaged T_2^* was determined by eliminating the first data points of the magnetization decays as described by Kriz et al.³⁷ Figure 11 shows the temperature dependence of T_2^* of samples **P1–P3**.

Figure 10 shows the T_1 data of different moieties of the hydrophobic and the hydrophilic blocks. This allows for detailed discussions of the dynamics of these parts of the polymers. In particular, the relaxation times of the side chain protons of the hydrophobic block as well as the COCH_3 and CH_2 protons of the hydrophilic block could be studied.

The T_1 data of Figure 10 show the same behavior for all three samples. While the T_1 temperature dependences of the hydrophobic block provide an increase of T_1 toward higher temperatures, the T_1 data of the hydrophilic parts show the opposite tendency. Furthermore, the magnitudes of the T_1 data differ for the structural groups of the side and the main chain, indicating the differences of the dynamics of the substructural groups of the hydrophobic and hydrophilic blocks. The end

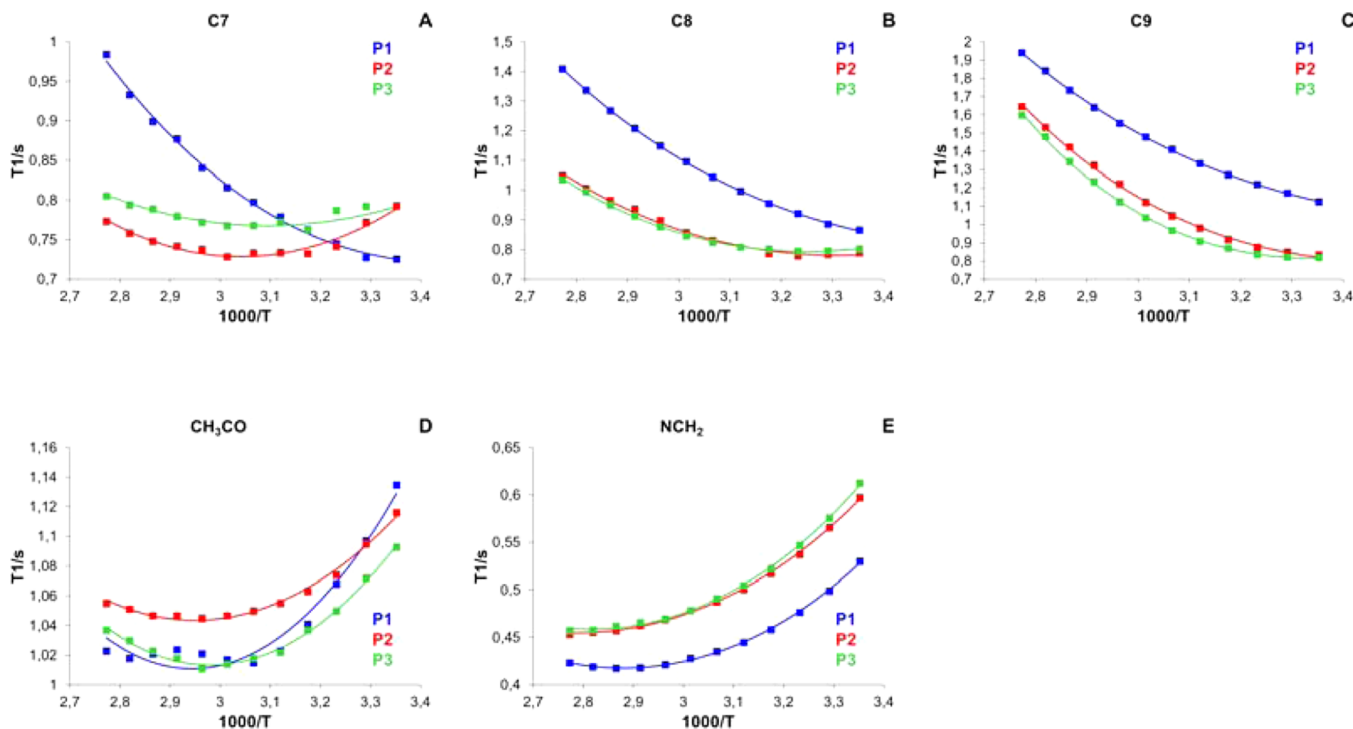


Figure 12. Temperature dependence of calculated (solid lines) and measured (■) T_1 relaxation times of samples P1 (blue), P2 (red), and P3 (green) at 500 MHz. The T_1 data were simulated with the BPP model for isotropic molecular reorientations.

groups C9 always deliver the largest T_1 followed by C8 and C7, and the NCH_2 groups provide the lowest T_1 values. These differences are caused by the fast mobility of the end groups and the restricted mobilities if coming closer to the backbone of the polymers. It was also found that the T_1 values of a certain side chain group differ for the three samples, namely that P1 shows the largest T_1 data followed by P2 and P3. The T_1 values are decreasing with increasing side chain lengths. In addition, some of the temperature dependences offer even a minimum. Differences of the T_1 behavior with increasing temperature are also observed for poly(*N*-isopropylacrylamide) in water.⁶¹ However, the different tendencies of T_1 are explained with respect to the LCST phase separation. Such LCST behavior seems not appearing in our measurements because no dramatic changes of the T_1 data are observed. The relaxation data of our samples continuously change with temperature.

The T_2 data of Figure 11 also provide similar results for the side chains as found for T_1 . The end groups C9 have the largest T_2 in comparison to C8 and C7. Furthermore, the same tendency was found as for T_1 by comparing the three copolymers for a certain group. The T_2 data are decreasing for the copolymers with increasing side chain lengths. However, the largest T_2 data were obtained for the COCH_3 group. It also should be noted that some of the temperature dependences of T_2 show a minimum as found for the hydrophobic side chain groups C7 and C8 for all samples and for C9 of sample P1 (see Figure 11). This behavior is in good agreement with the temperature dependence of T_2 of PEO-PPO-PEO triblock copolymers.⁴² In this case, the hydrophobic PPO block also shows a decrease of T_2 toward a minimum. This decrease is a result of the restricted movement of the hydrophobic block. Furthermore, Figure S14 shows also a significant amount of the short component of T_{2s} which can reach 70–95% in the temperature range of 25–50 °C for the side chain groups C7 and C8. These dominating short components of T_2 which are

also significantly shorter than the corresponding T_1 data are reflecting the rigid part of the micelle core. Such biexponential behavior is also observed in sodium dodecyl sulfonate in the presence of partially hydrolyzed polyacrylamide.⁶²

To describe the dynamics and the temperature dependence quantitatively, the T_1 and T_2 data were simulated with the theory of Bloembergen, Purcell, and Pound^{63–65} for isotropic rotational reorientations using an Arrhenius setup for the correlation time τ_c :⁶⁶

$$\frac{1}{T_1} = \frac{2}{3} M_2 \left[\frac{\tau_c}{1 + (\omega_0 \tau_c)^2} + \frac{4\tau_c}{1 + (2\omega_0 \tau_c)^2} \right] \quad (6)$$

$$\frac{1}{T_2} = \frac{1}{3} M_2 \left[3\tau_c + \frac{5\tau_c}{1 + (\omega_0 \tau_c)^2} + \frac{2\tau_c}{1 + (2\omega_0 \tau_c)^2} \right] \quad (7)$$

$$\tau_c = \tau_\infty \exp \left\{ \frac{E_a}{RT} \right\} \quad (8)$$

with τ_c the correlation time of the isotropic motion, $\omega_0 = 2\pi\nu_0$ ($\nu_0 = 500$ MHz, the frequency of the measurement), M_2 the second moment of the two spin system, τ_∞ the limiting correlation time of rearrangements, E_a activation energy, R the gas constant, and T the temperature in kelvin.

It turned out that the simplest motional model was the best description of the temperature dependence of T_1 . It should be noted at least that the first attempts of simulating the T_1 curves used actually a Fuoss-Kirkwood distribution⁶⁷ and also the Williams-Landel-Ferry equation⁶⁸ for the correlation times. However, the fitting of the width parameter of the Fuoss-Kirkwood distribution together with the Arrhenius equation delivered always $\beta = 1$, which finally corresponds to the BPP formula. The fitting with the WLF approach required too many parameters for the simulation without getting clear depend-

ences of the parameters for the glass transition and the limiting temperature T_∞ and τ_∞ parameters. This approach would require a complete T_1 curve with passing the minimum for all structural groups. Therefore, eqs 6 and 8 were finally used for the calculation of T_1 by fitting the parameters τ_∞ , E_a , and M_2 . The excellent quality of the fitting is shown in Figure 12, and the corresponding parameters are summarized in Table 2.

Table 2. Parameters Fitted for T_1 (with Eqs 6 and 8) and T_2 (with Eqs 7 and 8) for Samples P1–P3

sample/ group	$\tau_\infty \times 10^{-12}$, s (T_1)	$\tau_\infty \times 10^{-12}$, s (T_2)	E_a , kJ/mol (T_1)	E_a , kJ/mol (T_2)	$M_2 \times$ 10^9 , s $^{-2}$
P1					
C7	2.11	2.94	11.0	13.5	4.6
C8	1.06	0.03	12.0	26.1	4.1
C9	0.90	0.25	12.2	19.6	3.2
CH ₃ CO	4.19	3.33	10.9	11.9	3.3
NCH ₂	1.59	2.71	13.9	12.4	7.9
P2					
C7	2.39	0.20	12.0	23.9	4.5
C8	0.90	0.02	13.5	29.2	4.2
C9	0.16	0.04	17.0	25.8	4.1
CH ₃ CO	1.00	4.93	8.4	11.3	3.2
NCH ₂	2.96	2.67	12.5	13.0	7.3
P3					
C7	4.90	0.03	10.0	32.1	4.3
C8	0.73	0.02	14.3	30.4	4.2
C9	0.06	0.007	20.3	31.7	4.1
CH ₃ CO	5.68	6.16	9.9	11.0	3.3
NCH ₂	2.03	2.75	13.5	13.2	7.2

Figure 12 demonstrates the comparison of the theoretical and experimental T_1 temperature dependences of the individual substructures of the hydrophobic and hydrophilic blocks as the comparison for the different samples. These expansions clearly show the sensible differences which cannot be resolved in Figure 10. In particular, it can be seen that the side chain groups of the hydrophobic block show T_1 minima measured between ambient temperature (or lower) and 55 °C, whereas the NCH₂ and the CH₃CO groups of the hydrophilic group exhibit T_1 minima at higher temperatures (57–77 °C). These temperatures can be experimentally obtained from Figure 12 or theoretically predicted by the fitted functions. Table 3 shows

Table 3. Temperatures (in kelvin) of the T_1 Minima for Samples P1–P3

group	P1 (pentyl)	P2 (heptyl)	P3 (nonyl)
C7	(291.1)	328.9	326.7
C8	(277.0)	302.0	307.5
C9		(288.2)	299.7
COCH ₃	339.6	339.0	335.6
NCH ₂	347.3	358.8	355.6

the measured and predicted temperatures of the T_1 minima (predicted data in parenthesis with exception of C9 of P1 which predicts an unexpected high value). These temperatures accidentally correspond to the glass temperature T_g and melt temperature T_m of Table 4 if the side chains and the backbone minima are considered, respectively. It cannot be stated for sure that these minima are related to the dynamic glass transition. In the case of bulk samples these minima would appear at higher temperatures due to the high frequency of the measurements.

Table 4. Glass and Melting Temperatures (in kelvin) for Samples P1–P3 Measured with DSC

sample	T_g	T_m
P1	280.0	370.0
P2	306.8	365.0
P3	300.2	338.2

However, these T_1 measurements were performed in solutions where completely different mobilities are present compared to solid samples. Therefore, it might be possible that these minima somehow can be related to the dynamic glass transition, but this cannot be established now. In any case, all temperature dependences could be well described by the simple model of isotropic reorientations.

In the case of T_2 , the entire temperature dependences could only be fitted with the BBP model for the hydrophilic groups (COCH₃ and NCH₂) for all samples as well as for C9 for samples P2 and P3 (see Figure 13). The other temperature curves showed minima and could not be entirely simulated. Therefore, only the high temperature ranges were calculated for these cases. Table 3 shows the fitted parameters for τ_∞ and E_a by using the corresponding second moments of the T_1 simulations.

The values of Table 2 correspond to typical data of polymer solutions. The activation energies, for instance, are an order of magnitude smaller compared to bulk samples and agree well with data obtained for solutions of PEO–PPO–PEO, polystyrene, poly(methyl methacrylate), and poly(vinyl acetate).^{42,69–71} The values of τ_∞ are also in the range of the frequency limits (10¹²–10¹⁴ Hz) for molecular rearrangements and deliver magnitudes of the correlation times τ_c comparable to refs 42, 70, and 71. The temperature dependences of τ_c are plotted in Figures 14 and 15 for T_1 and T_2 , respectively. All polymers show the same tendency with respect to the mobility of the hydrophilic block (COCH₃ and NCH₂). These temperature dependences of the correlation times are very similar for T_1 and almost identical for the T_2 calculations. In particular, it was found that the backbone (NCH₂) provides the largest correlation times for T_1 , while in the case of T_2 these correlation times are significantly shorter than the correlation times of the side chains. This indicates that the hydrophilic block is much more flexible than the side chain of the hydrophobic block. It should be noted that the dynamics of the amphiphilic block copolymers refer to the nonaggregated parts of the polymer.

If only T_1 is considered, the smallest correlation times are found for C9, indicating the fastest motions of the end groups of the side chains. According to Figure 14, C9 of the side chain is moving faster than C8 followed by C7. Moreover, the CH₃CO group shows higher mobility than the NCH₂ group. These results are in agreement with the results of the aggregations. Considering the influence of the side chain lengths on the correlation times fitted from T_1 for a specific structural group, a slight increase of the correlation times is observed with the increasing chain length. This behavior is significantly more pronounced for T_2 . Figure 15 is demonstrating the strong effect of the side chain length. The correlations times of the hydrophobic block dramatically increase with the increasing side chain length. Moreover, the differences of the correlation times between C7, C8, and C9 are also much more expanding with increasing side chain lengths. These results are supporting the restricted mobility of the rigid core of the

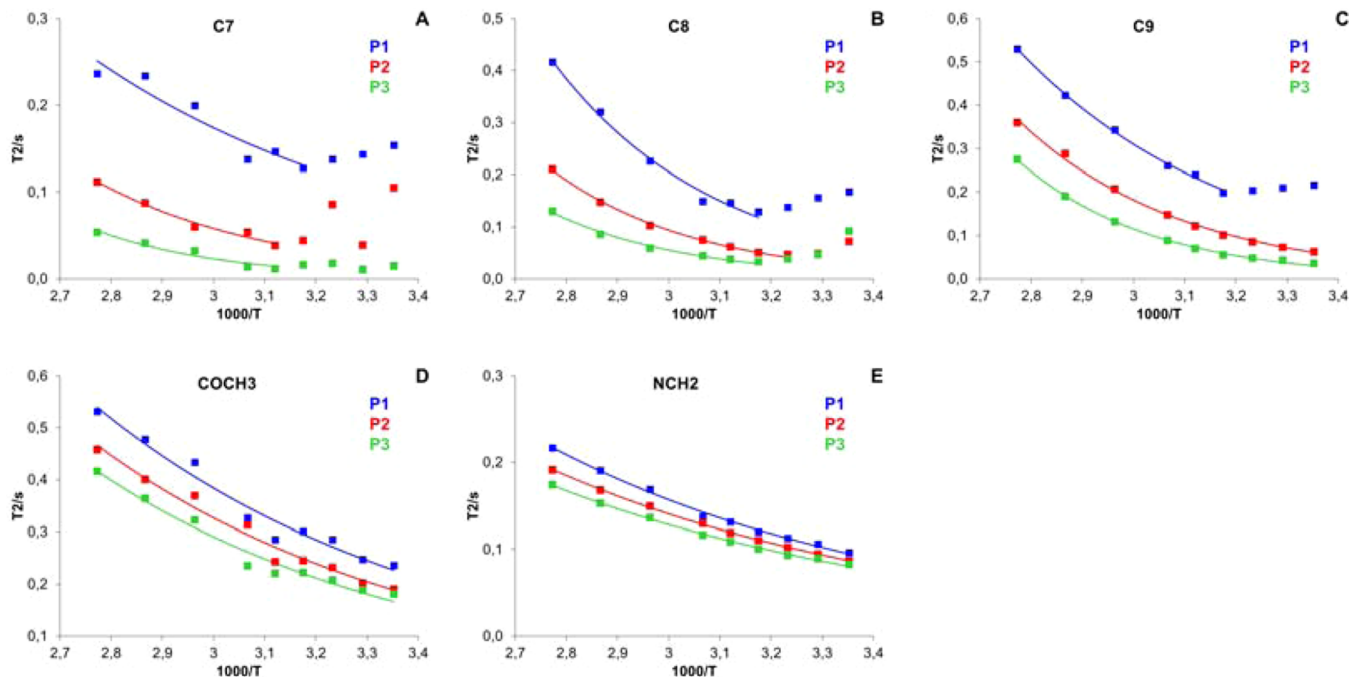


Figure 13. Temperature dependence of calculated (solid lines) and measured (■) T_2^* relaxation times of samples P1 (blue), P2 (red), and P3 (green) at 500 MHz. The T_2^* data were simulated with the BPP model for isotropic molecular reorientations.

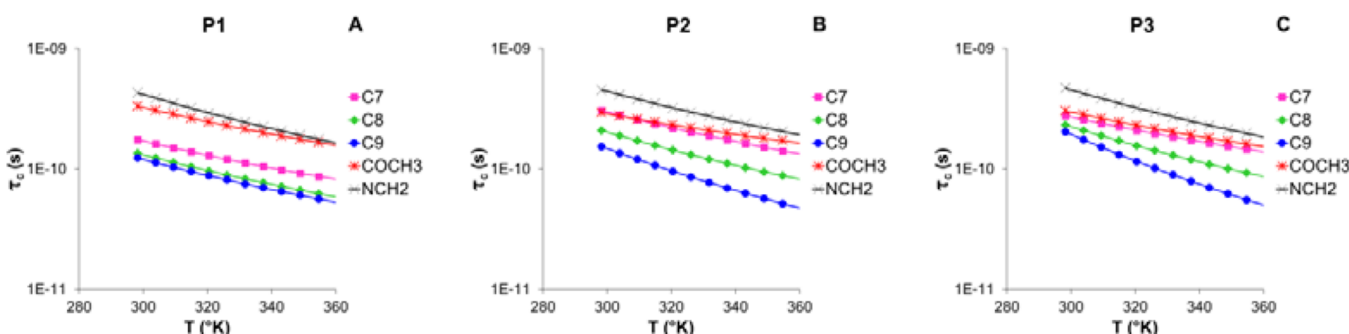


Figure 14. Temperature dependence of the correlation times τ_c of samples P1–P3 using τ_∞ and the activation energies of Table 2 obtained from the T_1 simulation.

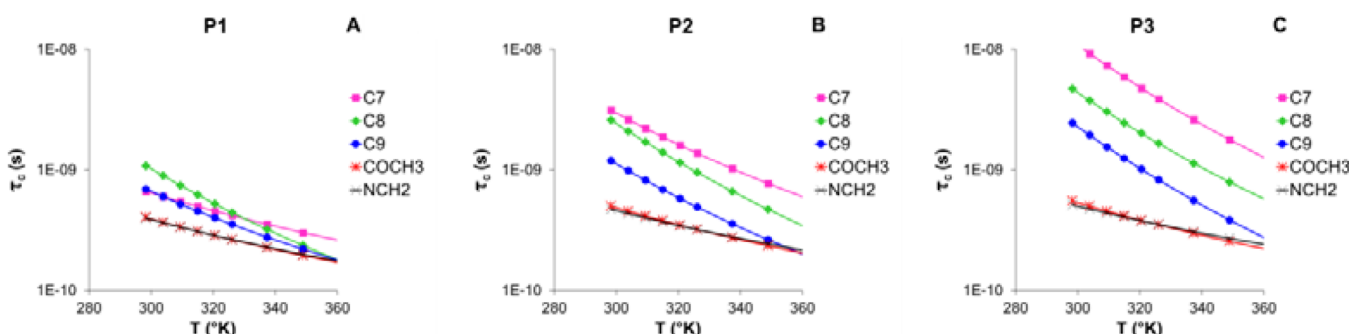


Figure 15. Temperature dependence of the correlation times τ_c of samples P1–P3 using τ_∞ and the activation energies of Table 2 obtained from the T_2 simulation.

hydrophobic block. The results from the temperature-dependent T_1 and T_2 analysis together with the quantification of aggregation from 3.1 suggest that the temperature-dependent increase in micellar size of P1 to P3 cannot be attributed to a cloud point temperature. The hydrophilic poly(2-methyl) blocks do not show any aggregate formation with increasing temperature as can be seen in Figure 9A–C, and the

hydrophobic side chain moieties display a decrease in aggregation with increasing temperature (also seen in Figure 9A–C) accompanied by an increase in T_1 values for the alkyl side chains (see Figure 12), indicating increased local mobility. Both results—the increasing signal intensity and local mobility with temperature—do not point to a typical LCST behavior,^{42,61} suggesting that this effect needs further

investigation and cannot be explained unambiguously based on our current data.

The activation energies E_a obtained from the T_1 and T_2 fittings are also in good agreement with ref 42. The E_a data of the hydrophilic blocks are in the range of 9–14 kJ/mol for all polymers. They show no differences for T_1 and T_2 . Differences are obtained for the hydrophobic structures. These energies are mainly in the range of 20–30 kJ/mol with the largest E_a values for **P3** with the highest hydrophobicity.

The fitted second moments are in the range of $(3\text{--}8) \times 10^9$ s⁻² and are in good confirmation with molten low molar mass PS behaving like liquids.⁷² Finally, it can be concluded that the dynamics of the individual groups of the hydrophilic and hydrophobic blocks can be quantified, and typical activation energies and correlation times are found.

CONCLUSIONS

In summary, we have analyzed the temperature-dependent micelle formation of three block copolymers based on poly(2-methyl-2-oxazoline)-*b*-poly(2-alkyl-2-oxazoline) with different alkyl side chains ranging from pentyl (**P1**) to heptyl (**P2**) to nonyl (**P3**). DLS measurements of the micellar solutions revealed particle sizes between 9.4 and 15.2 nm increasing with increasing side chain length. While the particles showed a temperature-sensitive behavior in the DLS measurements between 20 and 80 °C, the data showed that the particles were still present at 80 °C. Static fluorescence measurements and pyrene solubilization indicated between 20 and 80 °C a hydrophobic microenvironment for pyrene supporting the DLS data that the micellar aggregates are still intact at 80 °C. These micelles could be investigated in detail by NMR spectroscopy. Analysis of signal intensities allowed the determination of the degree of aggregation for the hydrophilic segment as well as different moieties of the hydrophobic side chain. While the hydrophilic polymer block does not show any aggregation the increasing side chain length causes an increase of the degree of aggregation for a considered structural hydrophobic group. The strength of these aggregations depends on the number of bonds of the individual group with respect to the backbone. The closer the investigated chemical group is attached to the polymer backbone, the stronger is the aggregation leading to a reduced mobility at the same time. Moreover, the longest side chain causes the strongest aggregations which cannot be completely dissolved within the studied temperature range. Analysis of polymer dynamics in the temperature range showed that the T_1 values of a certain structural group differ for the three samples, namely that **P1** always shows the largest T_1 values followed by **P2** and **P3**. The T_1 values are decreasing with increasing side chain lengths. The T_2 data provide similar results for the side chains as found for T_1 . The methyl end groups of the alkyl side chains have the largest T_2 in comparison to methylene groups. Furthermore, the same tendency was found as for T_1 by comparing the three copolymers for a certain group. The T_2 data are decreasing for the copolymers with increasing side chain lengths and the largest T_2 value were obtained for the COCH₃ group. The results are particularly interesting since they demonstrate on the one side the macroscopic stability of the micellar aggregates at higher temperature by DLS and fluorescence measurements and on the other side how the dynamics of the alkyl side chain where for example a ligand or catalyst can be immobilized depend strongly on the distance to the polymer backbone.

ASSOCIATED CONTENT

Supporting Information

Experimental details; Figures S1–S15. The Supporting Information is available free of charge on the ACS Publications website at DOI: 10.1021/acs.macromol.5b00149.

AUTHOR INFORMATION

Corresponding Authors

*E-mail Wolf.Hiller@tu-dortmund.de; Tel +49 (0) 231 755 3777 (W.H.).

*E-mail Ralf.Weberskirch@tu-dortmund.de; Tel +49 (0) 231 755 3863 (R.W.).

Notes

The authors declare no competing financial interest.

ACKNOWLEDGMENTS

P.D. is supported by the Cluster of Excellence RESOLV (EXC 1069) funded by the Deutsche Forschungsgemeinschaft

REFERENCES

- (1) Allen, P. E. M.; Downer, J. M.; Hastings, G. W.; Melville, H. W.; Molyneux, P.; Urwin, J. R. *Nature* **1956**, *177*, 910–912.
- (2) Bates, F. S.; Frederickson, G. H. *Annu. Rev. Phys. Chem.* **1990**, *41*, 525–557.
- (3) Discher, B. M.; Hammer, D. A.; Bates, F. S.; Discher, D. E. *Curr. Opin. Colloid Interface Sci.* **2000**, *5*, 125–131.
- (4) Discher, B. M.; Won, Y. Y.; Ege, D. S.; Lee, J. C. M.; Bates, F. S.; Discher, D. E.; Hammer, D. A. *Science* **1999**, *284*, 1143–1146.
- (5) Riess, G. *Prog. Polym. Sci.* **2003**, *28*, 1107–1170.
- (6) Kataoka, K.; Kwon, G. S.; Yokoyama, M.; Okano, T.; Sakurai, Y. *J. Controlled Release* **1993**, *24*, 119–132.
- (7) Kwon, G. S. *Crit. Rev. Ther. Drug Carrier Syst.* **2003**, *20*, 357–403.
- (8) Nishiyama, N.; Kataoka, K. *Pharmacol. Ther.* **2006**, *112*, 630–648.
- (9) Nakanishi, T.; Fukushima, S.; Okamoto, K.; Suzuki, M.; Matsumura, Y.; Yokoyama, M.; Okano, T.; Sakurai, Y.; Kataoka, K. *J. Controlled Release* **2001**, *74*, 295–302.
- (10) Allen, C.; Yu, Y. S.; Maysinger, D.; Eisenberg, A. *Bioconjugate Chem.* **1998**, *9*, 564–572.
- (11) Kwon, G.; Naito, M.; Yokoyama, M.; Okano, T.; Sakurai, Y.; Kataoka, K. *J. Controlled Release* **1997**, *48*, 195–201.
- (12) Elsabahy, M.; Wooley, K. L. *Chem. Soc. Rev.* **2012**, *41*, 2545–2561.
- (13) Hamley, I. W. In *The Physics of Block Copolymers*; Hamley, I. W., Ed.; Oxford Science Publications: Oxford, UK, 1998; Vol. 4, Chapters 3 and 4, pp 131–265.
- (14) Munch, M. R.; Gast, A. P. *Macromolecules* **1990**, *23*, 2313–2320.
- (15) Breulman, M.; Förster, S.; Antonietti, M. *Macromol. Chem. Phys.* **2000**, *201*, 204–211.
- (16) Klingelhoefer, S.; Heitz, W.; Greiner, A.; Oestreich, S.; Förster, S.; Antonietti, M. *J. Am. Chem. Soc.* **1997**, *119*, 10116–10120.
- (17) Zarka, M. T.; Nuyken, O.; Weberskirch, R. *Chem.—Eur. J.* **2003**, *9*, 3228–3234.
- (18) Liu, Y.; Pinon, V., III; Weck, M. *Polym. Chem.* **2011**, *2*, 1864–1975.
- (19) Kobayashi, S. *Prog. Polym. Sci.* **1990**, *15*, 751–823.
- (20) Kobayashi, S.; Uyama, H. *J. Polym. Sci., Part A* **2002**, *40*, 192–209.
- (21) Schlaad, H.; Diehl, C.; Gress, A.; Meyer, M.; Demirel, A. L.; Nur, Y.; Bertin, A. *Macromol. Rapid Commun.* **2010**, *31*, 511–525.
- (22) Aoi, K.; Okada, M. *Prog. Polym. Sci.* **1996**, *21*, 151–208.
- (23) Chiu, T. T.; Thill, B. P.; Fairchok, W. J. In *Water Soluble Polymers*; Advances in Chemistry Series 213; Glass, J. E., Ed.; American Chemical Society: Washington, DC, 1986; pp 425–433.
- (24) Chen, F. P.; Ames, A. E.; Taylor, L. D. *Macromolecules* **1990**, *23*, 4688ff.

- (25) Diab, C.; Akiyama, Y.; Kataoka, K.; Winnik, F. M. *Macromolecules* **2004**, *37*, 2556–2562.
- (26) Park, J.-S.; Kataoka, K. *Macromolecules* **2006**, *39* (19), 6622–6630.
- (27) Takahashi, R.; Sato, T.; Terao, K.; Qiu, X.-P.; Winnik, F. M. *Macromolecules* **2012**, *45*, 6111–6119.
- (28) Gaertner, F. C.; Luxenhofer, R.; Blechert, B.; Jordan, R.; Essler, M. *J. Controlled Release* **2007**, *119* (3), 291–300.
- (29) Luxenhofer, R.; Han, Y.; Schulz, A.; Tong, J.; He, Z.; Kabanov, A. V.; Jordan, R. *Macromol. Rapid Commun.* **2012**, *33*, 1613–1631.
- (30) Roßbach, B.; Leopold, K.; Weberskirch, R. *Angew. Chem., Int. Ed.* **2006**, *45*, 1309–1312.
- (31) Weberskirch, R.; Sand, H. *RSC Adv.* **2015**, *5*, 38235–38242.
- (32) Schönfelder, D.; Nuyken, O.; Weberskirch, R. *J. Organomet. Chem.* **2005**, *690*, 4648–4655.
- (33) Bortenschlager, M.; Schöllhorn, N.; Wittmann, A.; Weberskirch, R. *Chem.—Eur. J.* **2007**, *13*, 520–527.
- (34) Schönfelder, D.; Fischer, K.; Schmidt, M.; Nuyken, O.; Weberskirch, R. *Macromolecules* **2005**, *38*, 254–262.
- (35) Gall, B.; Bortenschlager, M.; Nuyken, O.; Weberskirch, R. *Macromol. Chem. Phys.* **2008**, *209* (11), 1152–1159.
- (36) Nivaggioli, T.; Tsao, B.; Alexandridis, P.; Hatton, T. A. *Langmuir* **1995**, *11*, 119–126.
- (37) Kriz, J.; Masar, B.; Plestil, J.; Tuzar, Z.; Pospisil, H.; Doskocilova, D. *Macromolecules* **1998**, *31*, 41–51.
- (38) Kriz, J.; Masar, B.; Pospisil, H.; Plestil, J.; Tuzar, Z.; Kiselev, M. A. *Macromolecules* **1996**, *29*, 7853–7858.
- (39) Kriz, J.; Masar, B.; Doskocilova, D. *Macromolecules* **1997**, *30*, 4391–4397.
- (40) Fleischer, G.; Bloss, P.; Hergeth, W. D. *Colloid Polym. Sci.* **1993**, *271*, 217–222.
- (41) Godward, J.; Heatley, F.; Booth, C. *J. Chem. Soc., Faraday Trans. 1995*, *91*, 1491–1496.
- (42) Cau, F.; Lacelle, S. *Macromolecules* **1996**, *29*, 170–178.
- (43) Heald, C. R.; Stolnik, S.; Kujawinski, K. S.; De Matteis, C.; Garnett, M. C.; Illum, L.; Davis, S. S.; Purkiss, S. C.; Barlow, R. J.; Gellert, P. R. *Langmuir* **2002**, *18*, 3669–3675.
- (44) Aramaki, K.; Olsson, U. *J. Colloid Interface Sci.* **2006**, *300*, 354–360.
- (45) Wilmes, G. M.; Arnold, D. J.; Kawchak, K. S. *J. Polym. Res.* **2011**, *18*, 1787–1797.
- (46) Zheng, C.; Huang, H.; He, T. *Macromol. Rapid Commun.* **2013**, *34*, 1654–1661.
- (47) Carr, H. Y.; Purcell, E. M. *Phys. Rev.* **1954**, *94*, 630–638.
- (48) Meiboom, S.; Gill, D. *Rev. Sci. Instrum.* **1958**, *29*, 688–691.
- (49) Trinh, L. T. T.; Lamberton-Thijs, H. M. L.; Schubert, U. S.; Hoogenboom, R.; Kjønksen, A. L. *Macromolecules* **2012**, *45*, 4337–4345.
- (50) Huber, S.; Hutter, N.; Jordan, R. *Colloid Polym. Sci.* **2008**, *286*, 1653–1661.
- (51) Jaksch, S.; Schulz, A.; Kyriakos, K.; Zhang, J. Q.; Grillo, I.; Pipich, V.; Jordan, R.; Papdakis, C. M. *Colloid Polym. Sci.* **2014**, *292*, 2413–2425.
- (52) Salzinger, S.; Huber, S.; Jaksch, S.; Busch, P.; Jordan, R.; Papdakis, C. M. *Colloid Polym. Sci.* **2012**, *290*, 385–400.
- (53) Bonné, T. B.; Lüdtke, K.; Jordan, R.; Stepanek, P.; Papdakis, C. M. *Colloid Polym. Sci.* **2004**, *282*, 833–843.
- (54) Kalyanasundaram, K.; Thomas, J. K. *J. Am. Chem. Soc.* **1977**, *99* (7), 2039–2044.
- (55) Engelhardt, N.; Ernst, A.; Kampmann, A.-L.; Weberskirch, R. *Macromol. Chem. Phys.* **2013**, *214*, 2783–2791.
- (56) Weber, C.; Hoogenboom, R.; Schubert, U. S. *Prog. Polym. Sci.* **2012**, *37*, 686–714.
- (57) Spevacek, J.; Schneider, B. *Makromol. Chem.* **1975**, *176*, 3409–3423.
- (58) Spevacek, J.; Schneider, B. *J. Polym. Sci., Polym. Lett. Ed.* **1974**, *12*, 349–350.
- (59) Spevacek, J. *J. Polym. Sci., Polym. Phys. Ed.* **1978**, *16*, 523–528.
- (60) Spevacek, J.; Hiller, W.; Hettrich, W.; Joel, D. *Eur. Polym. J.* **1989**, *25*, 1239–1243.
- (61) Zeng, F.; Tong, Z.; Feng, H. *Polymer* **1997**, *22*, 5539–5544.
- (62) Yuan, H.-Z.; S. Zhao, S.; Yu, J.-Y.; Shen, L.-F.; Du, Y.-R. *Colloid Polym. Sci.* **1999**, *277*, 1026–1032.
- (63) Bloembergen, N.; Purcell, E. M.; Pound, R. V. *Phys. Rev.* **1948**, *73*, 679–712.
- (64) Kubo, R.; Tomita, K. *J. Phys. Soc. Jpn.* **1954**, *9*, 888–919.
- (65) Abragam, A. In *The Principles of Nuclear Magnetism*; Clarendon Press: Oxford, 1961.
- (66) Ferry, J. In *Viscoelastic Properties of Polymers*, 3rd ed.; John Wiley: New York, 1980.
- (67) Fuoss, R. M.; Kirkwood, J. G. *J. Am. Chem. Soc.* **1941**, *63*, 385–394.
- (68) Williams, M. L.; Landel, R. F.; Ferry, J. D. *J. Am. Chem. Soc.* **1955**, *77*, 3701–3707.
- (69) Grandjean, J.; Sillescu, H.; Willenberg, B. *Makromol. Chem.* **1977**, *178*, 1445–1454.
- (70) Heatley, F.; Begum, A. *Polymer* **1976**, *17*, 399–408.
- (71) Heatley, F.; Cox, M. K. *Polymer* **1977**, *18*, 225–232.
- (72) Hiller, W.; Schenk, W. *Polymer* **1986**, *27*, 1353–1358.